

Control of separation on a trailing edge flap using air jet vortex generators

W.J.Crowther*
University of Manchester, UK

A primary design driver for current generation civil high lift systems is the retention of existing performance at lower overall cost. This paper considers the use of flow control to enable relaxation of flap geometric location constraints and hence increase value by reducing overall structural weight. The flow control model adopted is that of enhanced boundary layer mixing for effective camber recovery. This model predicts that performance is bounded with respect to flow control input by complete reattachment of the flow, and bounded with respect to flap deflection by advancement of the flap separation ahead of the flow control actuation location. Experimental work using a swept panel high lift model at a chord Reynolds number of 1.1×10^6 has identified that relaxation of the flap gap from $2.5\%c$ to $3.5\%c$ at a flap deflection of 37.5° led to an approximately 0.2 drop in C_L over the useful angle range. Surface pressure data and on and off-surface flow visualization studies have shown that this loss in performance is due to separation of the flap upper surface boundary layer. The application of flow control in the form of air jet vortex generators approximately $30\%x/c$ from the leading edge of the flap running at a velocity ratio of 2.6 enabled reattachment of the flap upper surface boundary layer and hence recovery of the original flap performance. Experiments at increased flap deflection demonstrated that the performance boundaries defined by the proposed flow control model are valid. Investigation of the effect of actuator spacing showed that a hole spacing ratio of 20 gave the best system gain. At experimental scale, results collapse reasonably well with speed using velocity or momentum ratio scaling. Provisional scaling of the experimental results to an A320 type aircraft indicate that approximately 0.5% of engine landing mass flow would be required based on velocity ratio scaling, and 8% based on momentum ratio scaling.

Nomenclature

A	=	Area
C_p	=	pressure coefficient
C_L	=	Lift coefficient
C_D	=	Drag coefficient
C_V	=	Jet velocity ratio
C_μ	=	Blowing coefficient (jet momentum ratio)
c	=	chord
D	=	Drag
DLG	=	Flap deflection, lap and gap
L	=	Lift
M	=	Mach number
n	=	Number of jets
p	=	Static pressure
p_o	=	Total pressure
q	=	Free stream dynamic pressure
S	=	Wing reference area
V	=	Speed
x/c	=	nondimensional distance measured in a chordwise sense

* Lecturer, School of Engineering, University of Manchester, Manchester, UK.

α	=	angle of attack, or jet skew angle
β	=	Jet pitch angle
Δ	=	Flap deflection
φ	=	Jet orifice diameter
γ	=	Ratio of specific heats
ρ	=	Density
λ	=	Jet orifice spacing

Subscripts

j	=	Jet
L	=	Local
∞	=	Free stream

Abbreviations

AJVG	Air Jet Vortex Generator
MEMS	MicroElectroMechanical Systems
VVG	Vane Vortex Generator

I. Introduction

Civil transport aircraft are typically optimized for high speed cruise, and as a result require a high lift system to obtain satisfactory performance at low speed¹⁻⁴. High lift system design probably reached its peak of complexity at the end of the 1960's in the 747, which needed a three-element (triple-slotted) trailing edge flap to get the required high lift performance. Since then, civil transport high lift systems have tended to become simpler, with many current generation high lift systems employing only a single element flap^{5,6}. The motivation for this is the pursuit of increased value through reduced manufacturing and maintenance costs rather than increased high lift performance. However, in order to achieve acceptable performance with a single element design, it is necessary to highly optimize the geometric location of the flap with respect to the main element trailing edge. This comes at the price of increased structural weight due to increased structural stiffness of the flap tracks and actuation system. Within the present work, it is proposed that by inclusion of flap flow control as part of the optimization process then equivalent performance can be achieved with relaxed geometric tolerances and therefore reduced weight and cost.

Traditional aerodynamic design is concerned with the arrangement of solid boundary conditions to optimize aerodynamic forces arising due to fluid flow. With the availability of flow control technologies⁷, the designer also has the freedom to modify aerodynamic as well as geometric boundary conditions. Aerodynamic boundary conditions are modified by injection of momentum tangential to the flow direction, e.g. circulation control via tangential blowing, or by providing means of redistributing the existing fluid momentum via the use of boundary layer mixing devices, e.g. vortex generators. Flow control devices such as vane vortex generators are routinely applied to production aircraft as flow fixes, and historically, circulation control has been applied to military high lift systems. However, as yet, integrated flow control technologies have not seen wide application on civil high lift systems, most probably due to the lack of suitable low-order models that can be used at the initial design stage.

The present work is part of the EU funded AEROMEMS II research program, involving collaboration between European industry and academia (see acknowledgements). The previous AEROMEMS I program was initiated in 1997 and identified actuator and sensor concepts that showed promise as practical MEMS flow control solutions. The aim of AEROMEMS II is the demonstration and evaluation of specific technologies on a civil transport high lift system at industrially relevant Reynolds number and Mach number. The primary role of the University of Manchester was in de-risking the full scale wind tunnel application of flow control on a trailing edge flap through prior demonstration at medium scale in a relatively low cost wind tunnel facility.

II. Flow control strategy and implementation

The flow control philosophy adopted in the present work is based on the enhancement of flap effectiveness through recovery of effective camber. By definition, if the flow is fully attached and the boundary layer is infinitely

thin, then the effective camber is equal to the geometric camber. For a boundary layer of finite thickness then the effective camber will generally be slightly less than the geometric camber, however, if the upper surface boundary layer is separated then the effective camber may be significantly reduced. Note that the flow control approach is based on the *recovery* of effective camber, i.e. the goal is to recover the performance lost due to adverse viscous effects. This is different to other more aggressive approaches, e.g. circulation control, which attempt to increase the effective camber above the geometric camber limit.

A schematic representation of the performance boundaries of a flap flow control scheme based on recovery of effective camber is shown in Fig. 1. The abscissa in this figure represents the chordwise location of the flap upper surface separation measured from the trailing edge, which is roughly equivalent to the strength of the separation. The ordinate represents the potential increase in effective camber that could be obtained from flow control devices based on boundary layer momentum redistribution. For fully attached flap flow, the potential gain in effective camber is limited by that which can be obtained from boundary layer thinning and thus is relatively small. As conditions give rise to movement of the flap separation towards the leading edge, the potential improvement to obtained from flow control increases. However a point is eventually reached where the separation moves ahead of the flow control actuation station, whereupon control effectiveness reduces to zero.

For the present work, flow control is effected by the application of Air Jet Vortex Generators (AJVGs) to the flap upper surface boundary layer near the leading edge. These devices enhance the mixing between the boundary layer flow and free stream through production of streamwise helical structures, and hence increase the momentum in the boundary layer close to the surface. In contrast to conventional Vane Vortex Generators (VVGs), AJVGs enable improved penetration of the vortices through severe adverse pressure gradients by pumping excess momentum along the core of the vortices⁸. AJVGs also have the advantage that they impose minimal drag penalty when not in operation.

A major issue concerning the application of VGs of either type is in choosing appropriate location, spacing and orientation⁹⁻¹⁵. An extensive parametric investigation of this problem was conducted by a partner in the AEROMEMS II research program, and the results of this are presented in refs 16, 17 and 18. There is general consensus amongst researchers that to be effective the AJVGs array must be located upstream of the region of flow to be controlled, and that the most effective orientation is a pitch angle of 45° and skew angle of 90° . In terms of the pros and cons of co or counter rotating arrays, the effect of hole size with respect to the boundary layer height, the spacing ratio of the holes with respect to the hole diameters, the picture is a little more mixed¹⁸. For the present work, the AJVG implementation parameters are shown in Table 1. The orifice diameter was chosen on the basis that it was the smallest hole that could be drilled without specialist equipment and was reasonably close to the minimum hole size proposed from a MEMS fluidic efficiency point of view¹⁹ (0.3mm). Note that the size of the orifices relative to the boundary layer thickness is large compared to typical values (e.g. 0.1) used for the optimization studies in ref. 18. The orifice spacing of 5mm was chosen on the basis of previous experimental work²⁰ on the model using VVGs that had shown a spacing of 10mm was effective. 5mm spacing allows testing at 10 and 20mm spacing through selective blocking of orifices. The VVG work had also shown that at a spacing of 10mm, a co rotating array was more effective than a counter rotating array.

Table 1 AJVG implementation parameters

<i>Fluid reference parameters</i>		<i>Geometric design parameters</i>		<i>Derived parameters</i>	
Typical local flow speed	60m/s	Orifice diameter, ϕ	0.5mm	Nondimensional orifice size, ϕ/δ	0.5
Typical local boundary thickness, d	1mm	Orifice spacing, λ	5mm	Orifice spacing ratio, λ/ϕ	10, 20, 40
Max jet speed	180m/s	Pitch angle, β	45°	Max jet velocity ratio	3
		Skew angle, α	90°		
		Rotation pairing	Co Rotating		

In order to obtain results in a timely manner it was decided to use ‘simulated’ MEMS AJVGs for the work at Manchester, i.e. compressed air would be supplied to an array of orifices drilled in to the upper surface of the flap via a common plenum chamber. The experiment retained relevance through use of orifice geometry and plenum pressure levels appropriate to the MEMS actuators under development. It was recognized that the ‘simulated’ AJVGs could only be run continuously, and as such, the anticipated efficiency gains obtained by pulsed blowing could not be evaluated.

III. Apparatus and experimental methods

A. Wind tunnel model

The model consists of a single wing and half a fuselage and was mounted to the roof of the wind tunnel with the wing orientated vertically downwards, Fig 2 and Fig.3. The wing has a semi-span of 1.194m, a constant flap stowed chord of 0.548m, and a sweep angle of 22.7°. The wing reference area is 0.654m² based on the product of semi span and flap stowed chord. The fuselage is 2.5m long and designed to provide representative flow around the root of the wing. Unless stated otherwise, all testing was carried out at a velocity of 30m/s, giving a Reynolds number based on flaps stowed chord of around 1.1×10^6 . The model has a three-element high lift system consisting of main element, flap and slat. The flap is of the single slotted Fowler type. When retracted, 66% of its 142mm chord lies within the flap cove. The flap is mounted on three brackets and can be set at a number of discrete deflection settings. For the present work settings of 33, 37.5, 39.3, 42.7, 45.6, 47.6 and 50.6 ° were used. The brackets allow continuously variable positioning in terms of lap and gap. The design ‘optimal’ settings for the flap are 33.1 ° deflection 0% lap and 2.5% gap. The slat, main element and flap of the baseline model are pressure tapped at a spanwise station approximately 40% outboard of the fuselage. For ease of reference in the present experiments, the geometric setting of the flap is denoted by the three component vector $DLG = [\Delta \text{ lap } \text{ gap}]$, where $\Delta \in \{33, 37.5\}$, $\text{lap} = 0$, and $\text{gap} \in \{2.5, 3.5\}$. The wind tunnel is a closed return facility with a maximum speed of 70m/s and a working section free stream turbulence level of less than 0.1% at speeds up to 60m/s. The working section is vented to atmosphere at the downstream end by a slot around its circumference.

An exploded view of the flap assembly developed for the present experiments is shown in Fig. 4, with details of the AJVG orifice array shown in Fig. 5. The default spacing ratio for most of the experimental work was 20. Note that the holes are drilled at an angle of 45° with the outlet pointing in an inboard direction. An initial design based on an integral plenum chamber suffered greatly from leakage at high blowing pressures. The present design solved this problem by using a self contained plenum. The system was calibrated wind off using hot wire anemometry. It was found that the measured peak jet velocity was within 5% of that predicted from isentropic expansion of the plenum pressure, and the velocity distribution along the array was uniform also to within 5%. Note that the modified flap is not instrumented with pressure tappings.

B. Data reduction

The dependent parameters of lift, drag and pressure were nondimensionalised in the normal manner:

$$C_L = \frac{L}{q_\infty S}, \quad (1)$$

$$C_D = \frac{D}{q_\infty S}, \quad (2)$$

$$C_p = \frac{p_L - p_\infty}{q_\infty}, \quad (3)$$

where

$$q_\infty = \frac{1}{2} \rho V_\infty^2. \quad (4)$$

Within the present work, two different independent parameters are used to characterise the actuation effort. The first is the jet velocity ratio, C_V , defined as the ratio of the jet velocity to the local free stream velocity in the region of the jet exit. The second is the blowing momentum coefficient, C_μ , defined as the ratio of the jet momentum to free stream reference momentum.

From isentropic flow theory

$$M^2 = \frac{2}{\gamma - 1} \left[\frac{p_o^{\frac{\gamma-1}{\gamma}}}{p} - 1 \right] \quad (5)$$

Using the subscript L to refer to conditions local to the jet exit, j for the jet and ∞ for the free stream, C_V is obtained as follows:

$$C_V = \frac{V_j}{V_L} = \frac{M_j}{M_L} = \left(\frac{p_{o,j}^{\frac{\gamma-1}{\gamma}} - p_L}{p_{o,\infty}^{\frac{\gamma-1}{\gamma}} - p_L} \right)^{\frac{1}{2}}, \quad (6)$$

Note that both the local and plenum pressures are required to obtain a true measure of the jet Mach number. Since the modified blown flap model was not pressured tapped, it was necessary to estimate the local pressure coefficient from baseline experiments with the original flap.

The momentum coefficient is defined as follows:

$$C_\mu = \frac{\rho_j n A_j V_j^2}{\frac{1}{2} \rho_\infty A_{ref} V_\infty^2} \quad (7)$$

If the flow is assumed to be incompressible (an invalid assumption at the highest blowing pressures used within this study) then

$$C_p = 1 - \left(\frac{V_L}{V_\infty} \right)^2, \quad (8)$$

and hence

$$V_\infty = \frac{V_L}{\sqrt{1 - C_p}}. \quad (9)$$

Substitution of this result into (7) yields an expression relating the velocity ratio and momentum coefficients in terms of the local static pressure coefficient:

$$C_\mu = \frac{\rho_j n A_j (1 - C_p)}{\frac{1}{2} \rho_\infty A_{ref}} C_V^2 \quad (10)$$

IV. Results

C. Wind tunnel model baseline performance

Lift and drag characteristics with angle attack for the wind tunnel model for three different flap configurations are shown in Fig. 6. The three flap configurations are the design ‘optimal’ case of [33 0 2.5], an increased flap deflection case at the same lap and gap, [37.5 0 2.5], and, finally, an increased deflection case with increased gap, [37.5 0 3.5]. Overall, the results for all three cases are relatively similar and in keeping with the typical results expected for the given configuration. Of particular note is the abrupt stall at 28° angle of attack. Pressure plotting has shown that this stall precipitated by flow separation on the slat. Within the nominally linear range of the lift curve (0 – 25° angle of attack), some differences between the cases may be noted. Firstly, the [37.5 0 2.5] case shows a modest increment in C_L compared to the design optimal case. More importantly, the [37.5 0 3.5] case shows a small but significant *reduction* in C_L . This decrease is not uniform, showing two distinct dips at around 5 and 15° angle of attack.

As a means to understanding why the increase in flap gap leads to a reduction in flap performance, Fig. 7 shows the surface pressure around the slat, main element and flap for both the [37.5 0 2.5] case and the [37.5 0 3.5] case for 0, 5 and 10° angle of attack. Considering the LH column first (gap = 2.5), it can be seen that as the angle of attack increases, the load on the slat and main element increases, however the load on the flap remains approximately constant. This is in keeping with what would be expected since the main element induces a constant local angle of attack in the vicinity of the flap. Looking carefully at the upper surface pressures towards the rear of the flap, it can be seen that there is a zero pressure gradient region for about 20% x/c . This is indicative of local separation at around 80% x/c . Moving now to the relaxed gap case in the RH column, it can be seen that the slat and main element pressure distributions are similar to the optimal gap case. However, the trailing edge separation on the flap is much more pronounced, and in particular, for the $\alpha=5^\circ$ case, the separation has moved to the leading of the flap leading to complete flap stall. The resulting reduction in pressure loading over the main element correlates well with the observed loss in lift at $\alpha=5^\circ$ in Fig. 6.

On the basis of the above results, the [37.5 0 3.5] case was chosen as a test case for the application of flow control, with the goal being to try to recover the lift performance lost due to the increase in flap gap by application of AJVGs on the flap.

D. Flow control results

As a demonstration of the basic effectiveness of AJVGs in recovering the flap performance lost due gap relaxation, Fig. 8a shows the lift curve for the [37.5 0 3.5] case for no blowing and blowing at a C_V of 2.6. (Note that from results that will be shown later, it is known that a C_V of 2.6 is sufficient to saturate the control response). This latter blown case is then compared to the baseline unblown ‘optimal’ gap setting case in Fig. 8b. Note that the unblown baseline case in Fig. 8a does not show the larger dips in C_L at 5 and 15° angle of attack shown in Fig. 6. It is believed that this is due to small differences in flap geometry resulting from installation of the plenum chamber in the upper surface. Overall, these results clearly show that the flap performance has been substantially recovered by the application of blowing.

To establish a more detailed picture of the effectiveness of the AJVGs, tests were performed for range of flap deflections up to 51° and for C_V values up to 2.8 at 0, 5 and 10° angle of attack, the results of which are shown in Fig. 9. The results for each of the angles of attack are all similar in form. For lower flap deflections, increasing C_V increases the overall lift of the configuration, however, above a certain flap deflection, increasing C_V has zero effect, indicating that the flap separation has moved ahead of the actuator array. This behavior is consistent with the upper and right hand performance boundaries defined in Fig. 1.

Fig. 10 shows the lift to drag ratio of the model as a function of flap deflection for varying blowing at zero angle of attack. With no blowing, there is a general trend of decreasing L/D as the flap deflection is increased, as might be expected. With blowing applied, the L/D is improved for all flap deflections up to around 48°. This is consistent with the range over which blowing improves C_L , as shown in Fig. 9a. The best improvement in L/D is approximately 20% and occurs around 46° flap deflection. However note that the present flap configuration is typical of that used for landing and as such drag is not a major issue.

The effect of free stream speed and jet orifice spacing on the blown performance of the model is shown in Fig. 11. The LH column shows C_L plotted against C_V and the RH column shows C_L plotted against C_μ . Considering the C_V results first, it can be seen that the overall form of the results is similar for different speeds, particularly 20 and

30m/s. This confirms that it is reasonable to use C_V as a similarity parameter for the present work. Looking now at the effect of orifice spacing, it is clear that a spacing ratio of 20 produces results with the highest gain, i.e. the largest change in C_L for a given C_V , with the spacing ratio of 10 in second place. According to the model proposed in section II, the maximum effectiveness is effectively limited by complete reattachment of flow on the flap, and thus should be independent of orifice spacing. The results presented here tentatively support this, however further data at high C_V and high free stream speed is needed to reach a definite conclusion.

The results plotted against C_μ are a little harder to interpret since changing the spacing changes the overall orifice area and therefore changes C_μ for a given velocity ratio, however they give an indication of comparative gain of the various spacings based on the amount of momentum required. Once again it appears that the spacing ratio of 20 gives the best gain, however, interestingly the spacing ratio of 40 comes in second place. From a momentum perspective, it is clearly more efficient to use fewer orifices running at high C_V than it is to use more orifices running at low C_V .

E. Flow visualization

Surface oil flow visualization results comparing the flap upper surface flow pattern for blowing on and blowing off for the [37 0 3.5] test case are shown in Fig. 12. Considering the unblown case first, Fig. 12a, it can be deduced that the flow separates approximately $5\%x/c$ downstream from the jet orifice array. With blowing applied, Fig. 12b, the separation line has moved back to approximately $90\%x/c$ from the leading edge. This figure also shows evidence of streakline downstream of the jet orifices, typical of the patterns that would be expected for a longitudinal vortex embedded in the boundary sub-layer. These surface streaklines curve in a direction spanwise towards the wing tip eventually asymptoting to the separation line. This behavior is consistent with previous studies of vortex generating devices ahead of a 3d separation line.

A series of flow visualization images similar to those shown in Fig. 12 were obtained for a range of C_V values and free stream speed, and measurements made of the mean location of the flap upper surface separation location, Fig. 13. This figure clearly demonstrates two things. Firstly, it confirms that C_V is an appropriate similarity parameter for correlating separation location as a function of blowing input. Secondly, when compared with Fig. 11a-c, it can be seen that there is a direct correlation between flap separation location and overall C_L as would be expected from the flow control model presented in section 2.

Figure 14 shows a comparison of PIV-computed streamlines for the blown and unblown [37 0 3.5] case. Note that the PIV measurement plane is normal to the wing planform and aligned with the free stream. In the separated wake regions downstream of the main element and flap, the flow is both unsteady and has a strong outboard spanwise component. This means that the velocities in the PIV plane are relatively small and poorly correlated over time, and for this reason are excluded from the data set. This, and the finite resolution of the PIV camera, mean that it is not possible to ascertain the flow directly associated with the jet array. Note that the streamline spacing is computed based on an equal volume flow rate between each streamline, hence the streamlines are more closely spaced where the flow velocity is high.

Considering the unblown case first, Fig. 14a, it can be seen that regions of uniform high velocity flow exist at the top and bottom of the figure. The top region is the free stream flow outside of the slat/main element boundary layer, and the lower region is the free stream region outside the flap lower surface boundary layer. Note that the direction of the high speed flows above the main element and below the flap is relatively close to the free stream direction. There also exists a relatively large wake downstream of the flap and there is little indication of the jet like flow expected between the main element trailing edge and the nose of the flap. Taken together, this evidence suggests that the flow over the flap is largely separated, in keeping with the evidence from the surface flow visualization, force, and pressure data.

Considering now the blown case, Fig. 14b, a number of distinct changes may be noted in the flow field. Firstly, that the size of the wake downstream of the flap is reduced, secondly that the mean direction of the flow downstream of the flap and main element is more in line with the chordline of the flap, and lastly that there now exists a distinct jet like flow emanating from the gap between the main element and flap. This evidence suggests that the separation on the upper surface of the flap is moved downstream by the action of the AJVGs, which is compatible with the evidence from the force and surface pressure data.

V. Scaling considerations

The practicality of flow control schemes using blowing often hinges on the amount of engine bleed air required for their operation. In order to put experimental air requirements in to context, what follows is an approximate calculation of the engine bleed requirements if the present experimental rig was scaled up in size and speed to an

Airbus A320 aircraft, Table 2. The choice of aircraft is significant in that the A320 has a single element trailing edge flap, however, the stretched version of this aircraft (A321) required a double element trailing edge flap in order to meet low speed requirements. It is possible that with the judicious application of flow control to the original A320 flap, then the requirements of the A321 could have been met without the considerable additional expense of a double element flap. The bleed air requirements are calculated using two different methods. The first method is based simply on using the same hole diameter, spacing and velocity ratio on the full scale flap as on the model flap. The second method is based on the assumption that the momentum requirements can be scaled for a different wing area and free stream speed using the blowing coefficient. A maximum jet exit velocity of 280m/s ($M = 0.82$) is imposed as a constraint in both cases. Values are calculated approximately using equation 10 under the assumption of incompressible flow.

The results for the velocity ratio scaling and for momentum ratio scaling are presented in Tables 3 and 4, respectively. The input values for the calculation are in italics and the significant output values are in bold. A jet velocity ratio of 2 is chosen as a representative value from the present experimental work. This corresponds with a blowing coefficient of 0.00115 at 30m/s, model scale, and a hole spacing ratio of 20. If the results are scaled simply by velocity ratio, then an A320 scale application of the present flap flow control scheme would require a mass flow equal to 0.46% of the available engine mass flow and a momentum flow equal to 0.21% of the overall thrust during landing. Alternatively, if the results are scaled by momentum ratio, then the requirement would be a mass flow equal to 7.65% of the available engine mass flow and a momentum flow equal to 3.45% of the overall thrust for the same condition. Note that in order to keep the jet velocity below 280m/s for the momentum scaling case, it has been necessary to greatly increase the hole size beyond what is likely to be practical.

Whilst the above method of calculation is very rudimentary, the results highlight the importance of identifying the correct scaling parameters for work involving pneumatic flow control devices such as AJVGs. Clearly, if the flow control mechanism is based on a velocity ratio scaling then application at scale speed is likely to require far less engine air than if the mechanism is momentum based. In reality, the mechanism can not be wholly based on velocity ratio since this would imply that infinitely small jets would be infinitely efficient. As a result, the exact nature of the scaling is likely to involve a number of dimensionless parameters including those based on velocity and momentum ratios. The work presented in this paper has shown that AJVGs are effective reattaching separated flap flow. Understanding the exact nature of the scaling will be a necessary step in steering the technology towards commercial applicability.

Table 2 Reference data for the Airbus A320

Gross weight	74000kg
Wing span	34m
Wing reference area	122m ²
%span of trailing edge flap	80%
Power plant	CFM56-5, 120kN thrust
Number of engines	2
Mass flow per engine at take off	386kg/s
Mass flow per engine, landing	38.6kg/s
Approach speed	70m/s
Local C_p on flap at around 30% x/c	-3

Table 3 Blown air requirements based on jet velocity ratio scaling

jet velocity ratio	2	jet velocity	280m/s
orifice diameter	0.5mm	jet mass flow	0.18kg/s
hole spacing ratio	20	jet momentum	50.3N
orifice spacing	10mm	jet mass flow as a % of engine mass flow, landing	0.46%
total number of jets on flap	2720	jet momentum as a % of engine thrust, landing	0.21%
total orifice area	$5.34 \times 10^{-4} \text{m}^2$		

Table 4 Blown air requirements based on jet momentum coefficient scaling

jet momentum coefficient	0.00115	jet velocity	280m/s
orifice diameter	8.23mm	jet mass flow	2.95kg/s
hole spacing ratio	20	jet momentum	827N
orifice spacing	160mm	jet mass flow as a % of engine mass flow, landing	7.65%
total number of jets on flap	661	jet momentum as a % of engine thrust, landing	3.45%
total orifice area	$5.34 \times 10^{-4} \text{m}^2$		

VI. Conclusion

This paper has outlined the design requirements for civil transport high lift systems and made a case that value could be increased by the use of flow control to allow relaxation of the high lift system positional tolerances without loss in overall performance. The flow control model adopted is that of effective camber recovery through enhanced boundary layer mixing. This model predicts that performance is bounded with respect to flow control input by complete reattachment of the flow, and bounded with respect to flap deflection by advancement of the flap separation ahead of the flow control actuation location. Experimental work using a swept panel high lift model has identified that relaxation of the flap gap from $2.5\%c$ to $3.5\%c$ at a flap deflection of 37.5° led to an approximately 0.2 drop in C_L over the useful angle range of the high lift system. Surface pressure data and on and off-surface flow visualization studies have shown that this loss in performance is due separation of the flap upper surface boundary layer. The application of flow control in the form of AJVGs approximately $30\%x/c$ from the leading edge of the flap running at a C_V of 2.6 enabled reattachment of the flap upper surface boundary layer and hence recovery of the original flap performance. Experiments at increased flap deflection demonstrated that the performance boundaries defined by the proposed flow control model are valid. Investigation of the effect of actuator spacing showed that a hole spacing ratio of 20 gave the best system gain. At experimental scale, results collapse reasonably well with speed using C_V or C_μ as the similarity parameter. Provisional scaling of the experimental results to an A320 type aircraft indicate that approximately 0.5% of engine landing mass flow would be required based on a velocity ratio scaling, and 8% based on momentum ratio scaling.

Acknowledgments

The research reported here was undertaken as part of the AEROMEMS II project (Advanced Aerodynamic Flow Control using MEMS, Contract No. G4RD-CT-2002-00748). The AEROMEMS II project is a collaboration between BAE SYSTEMS, Dassault, Airbus Deutschland GMBH, EADS-Military, Snecma, ONERA, DLR, LPMO, The University of Manchester, LML, Warwick University, TUB, Cranfield University, NTUA and Auxitrol. The project is funded by the European Union and the project partners. Thanks are extended to Tim Harrison for providing the baseline wind tunnel data and Steven Kendall for the blown data.

References

- ¹Smith, A.M.O. "High-Lift Aerodynamics", AIAA Paper 74-939 (1974)
- ²Butter, D.J. "Recent Progress on Development and Understanding of High-Lift Systems", AGARD CP365 paper 1, pp. 1-1 to 1-26 (1984)
- ³Flaig A. and Hilbig R., "High-lift design for large civil aircraft," AGARD-CP-515, September 1993, Section 31, ISBN 92-835-0715-0.
- ⁴Rudolph, P.K.C. "High-Lift Systems on Commercial Subsonic Transport Aircraft" , NASA CR-4746. (1996)
- ⁵Wedderspoon, J.R. "The High Lift Development of the A320 Aircraft", Proceedings ICAS-86, pp. 343 – 351 (1986)
- ⁶Hansen, H., "Overview about the European High Lift Research Programme Eurolift", *AIAA 2004-767*.
- ⁷Gad-El-Hak, M., "Introduction to Flow Control", in Flow Control-Fundamental and Practices, Mohammed Gad-El-Hak, Andrew Poolard, Jean-Paul Bonnet, LNPM53, Springer Verlag, 1998, pp 1-107.
- ⁸Lewington, N.P., Peake, D.J., Henry, F.S, Singh, C., "Analogue/Digital Wind Tunnel Testing of Active Low Momentum Flow Control on Single and Multi-Component Airfoil Systems at High Lift," AIAA-2002-0303.
- ⁹Lin J. C., "Review of research on low-profile vortex generators to control boundary layer separation," Progress in Aerospace Science, Vol.38, No. 4-5, pp. 399 – 401.
- ¹⁰Suzuki T., Nagata M., Shizawa T., Honami S., "Optimal injection conditions of a single pulsed vortex generator to promote cross-stream mixing," Experimental Thermal and Fluid Science, 1998, vol. 17, pp. 139 – 146.
- ¹¹Selby G., Lin J. and Howard F., "Jet vortex generators for turbulent flow separation control," Symposium on Turbulence, 24th –26th September 1990.
- ¹²Magill J. C. and McManus K. R., "Exploring the feasibility of pulsed jet separation control for aircraft configurations,"
Journal of Aircraft, Vol. 38, No. 1, January-February 2001.
- ¹³Rae A. J., Galrin S. A. and Fulker J., "Investigation into the scale effects on the performance of sub boundary layer vortex generators on civil aircraft high-lift devices," 1st AIAA Flow Control Conference, 24th –26th June 2002.
- ¹⁴Lin J. C., "Review of research on low-profile vortex generators to control boundary layer separation," Progress in Aerospace Science, Vol.38, No. 4-5, pp. 399 – 401.
- ¹⁵Barberopoulos A. A., Garry K. P., "The effect of skewing on the vorticity produced by an airjet vortex generator," The Aeronautical Journal, March 1998, pp. 171 – 177.
- ¹⁶Godard, G., Stanislas, M., "Control of a decelerating boundary layer. Part 1: Optimization of passive vortex generators," AIAA Journal, submitted for publication Dec 2004.
- ¹⁷Godard, G., Stanislas, M., "Control of a decelerating boundary layer. Part 2: Optimization of slotted jets vortex generators," AIAA Journal, submitted for publication Dec 2004.
- ¹⁸Godard, G., Foucaut, J.M., Stanislas, M., "Control of a decelerating boundary layer. Part 3: Optimisation of round jets vortex generators," AIAA Journal, submitted for [publication](#) Dec 2004.
- ¹⁹Ho C. H, Tai Y. U., "Micro-Electro-Mechanical-Systems (MEMS) and fluid flow," Annual Review Fluid Mech., 1998, 30:579-612.
- ²⁰Harrison, T., "Separation Control on High-lift Systems Using Vane Vortex Generators", PhD Thesis, University of Manchester, 2005.

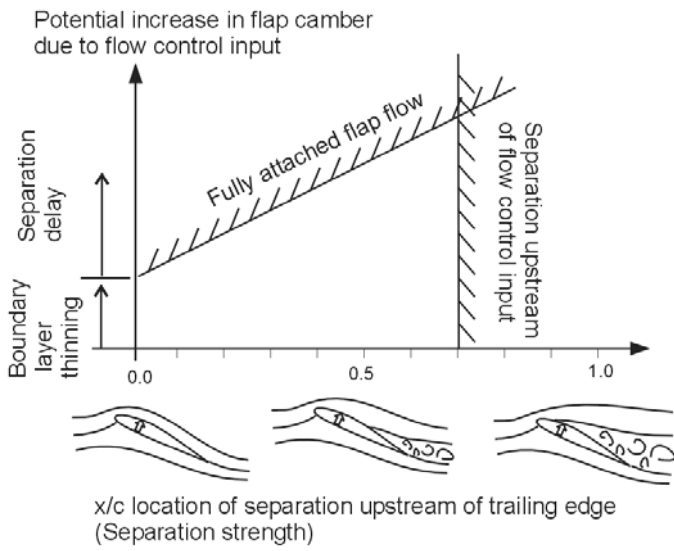


Figure 1 Schematic representation of the performance boundaries of a flap flow control scheme based on recovery of effective flap camber

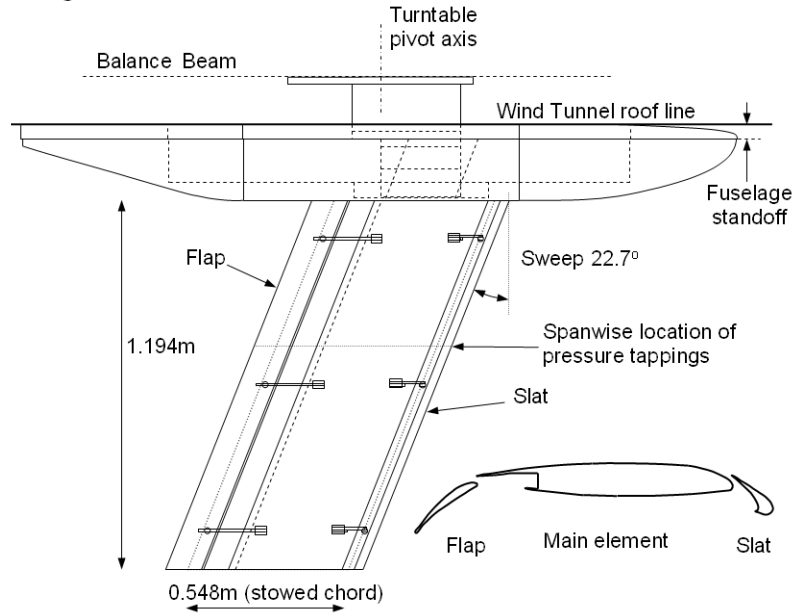


Figure 2 Geometric details of the N56 swept panel high lift model

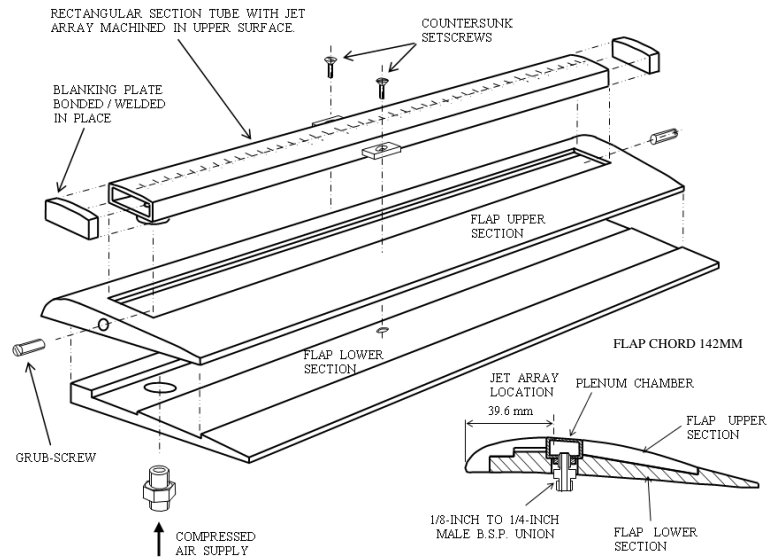


Figure 4 General arrangement of the trailing edge flap assembly with self-contained plenum chamber

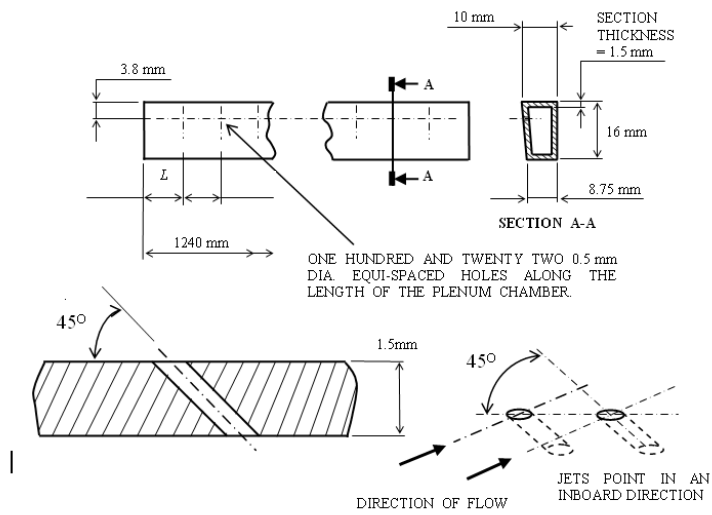


Figure 5 Air jet vortex generator array

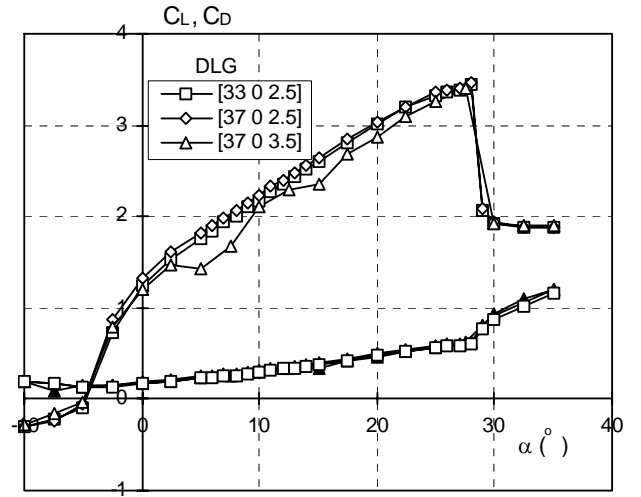


Figure 6 Lift and drag characteristics for the baseline (gap=2.5) and relaxed flap gap (gap=3.5) cases

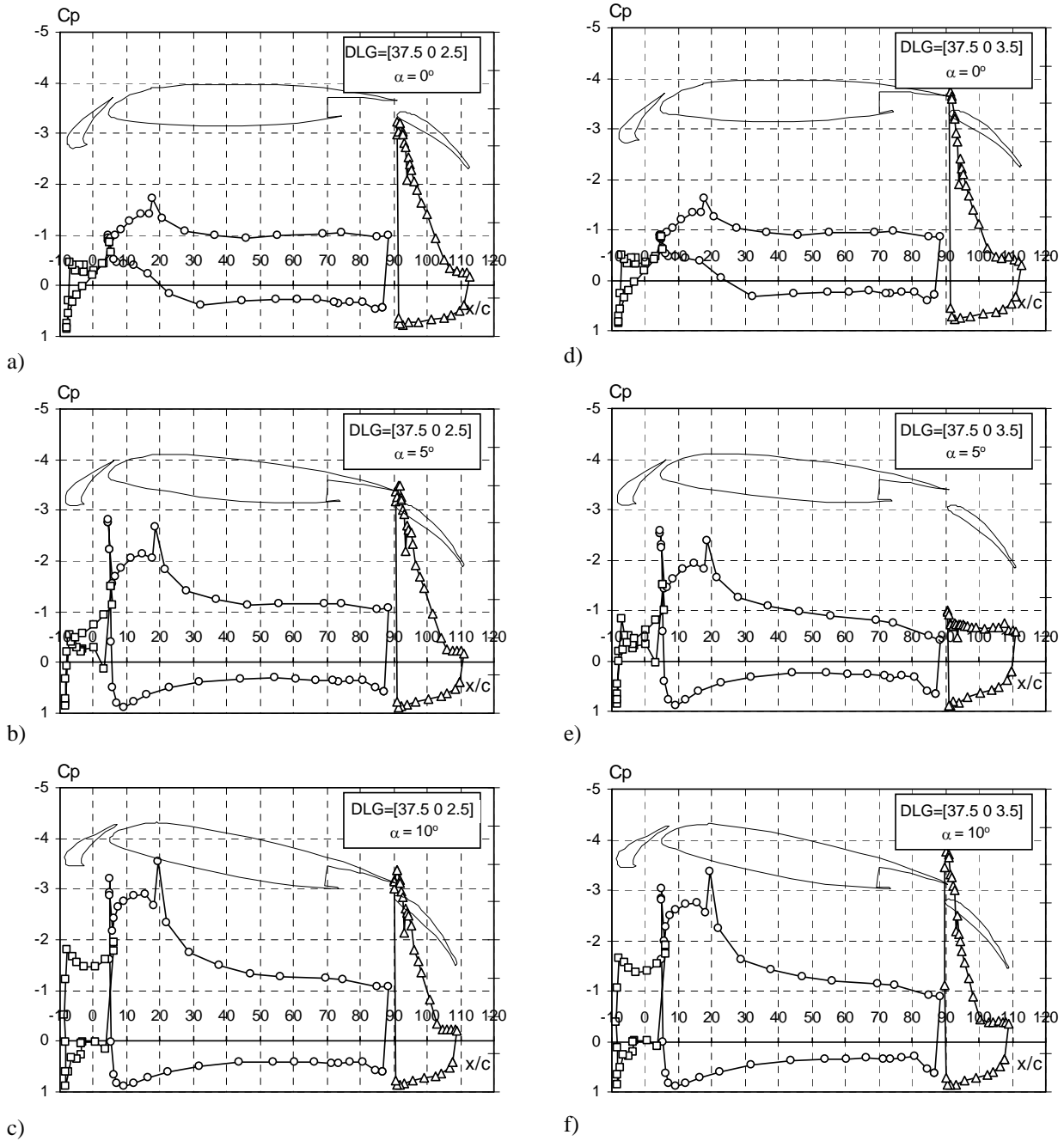
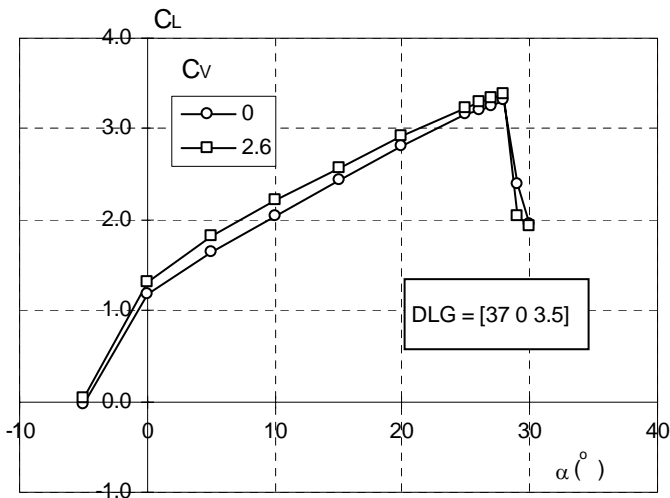
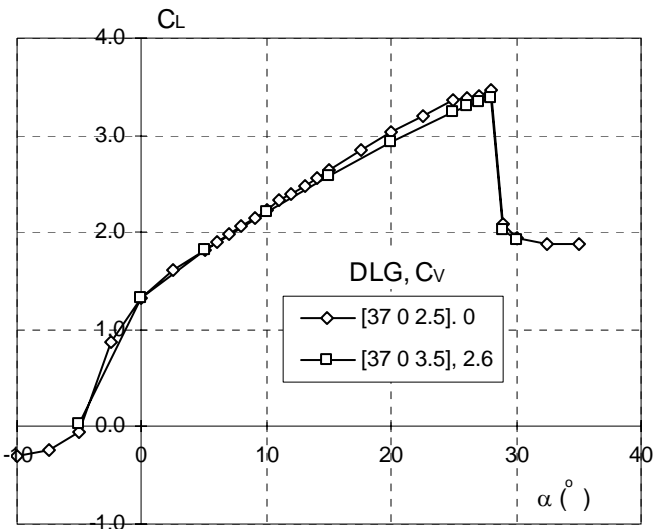


Figure 7 Slat, main element and flap pressure distributions for the baseline (LH column) and relaxed flap gap cases (RH column), $\alpha = 0, 5$ and 10° . x/c values are projections of the model x axis on to the wind axis.

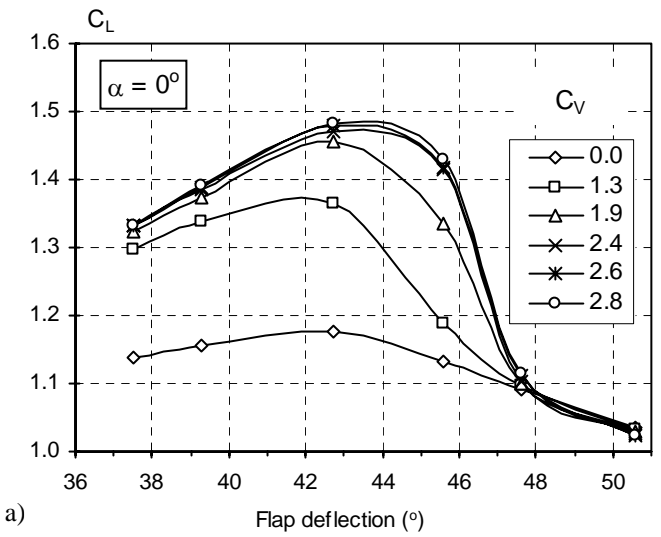


a) Recovery of relaxed flap gap wing performance due to blowing (modified flap)

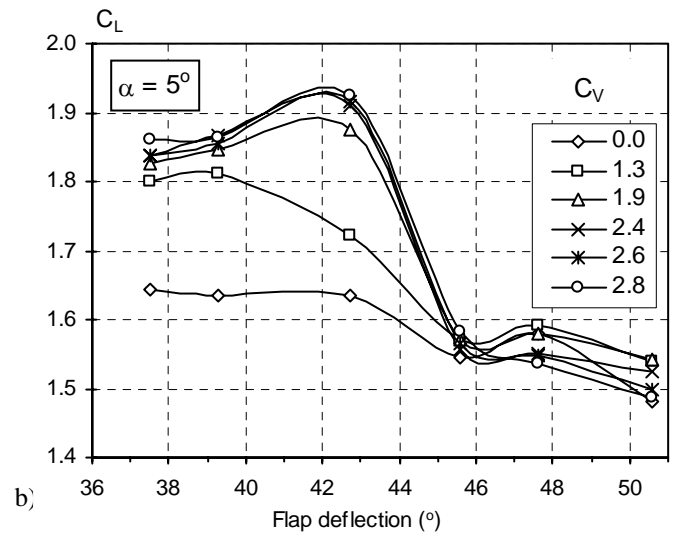


b) Comparison of optimal flap gap case with blown relaxed gap case

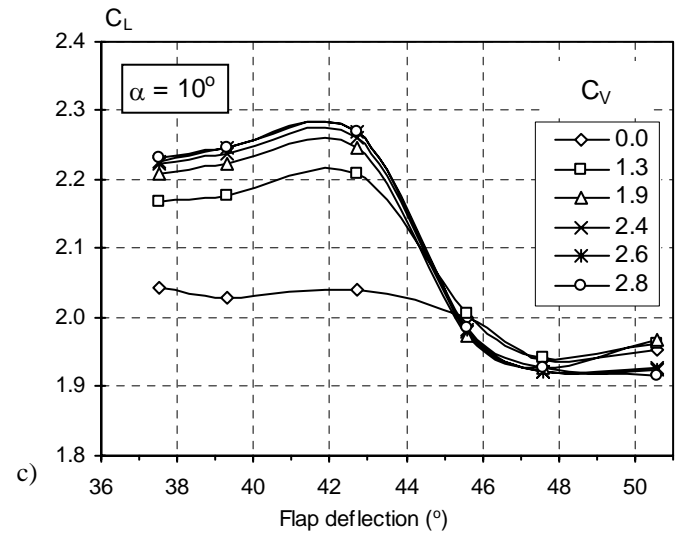
Figure 8 Demonstration of the effectiveness of AJVGs in recovery flap performance lost due to gap relaxation



a)



b)



c)

Figure 9 Flap performance recovery due to blowing for increasing flap deflection at 0, 5 and 10° angle of attack

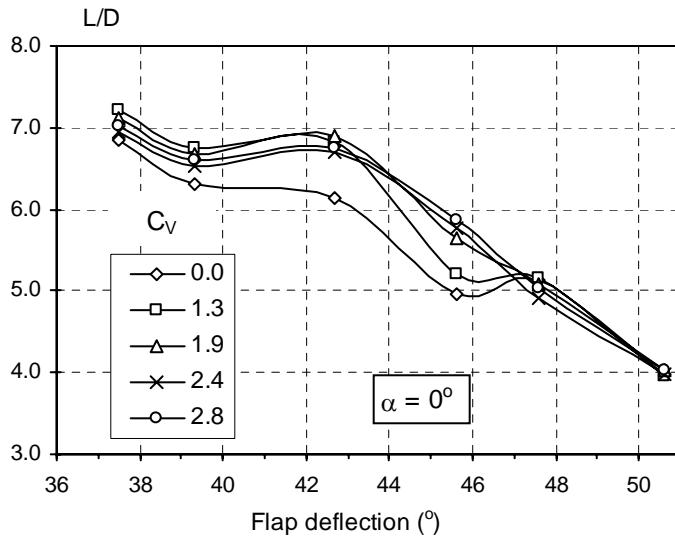


Figure 10 Lift to drag ratio as a function of flap deflection for varying jet velocity ratio

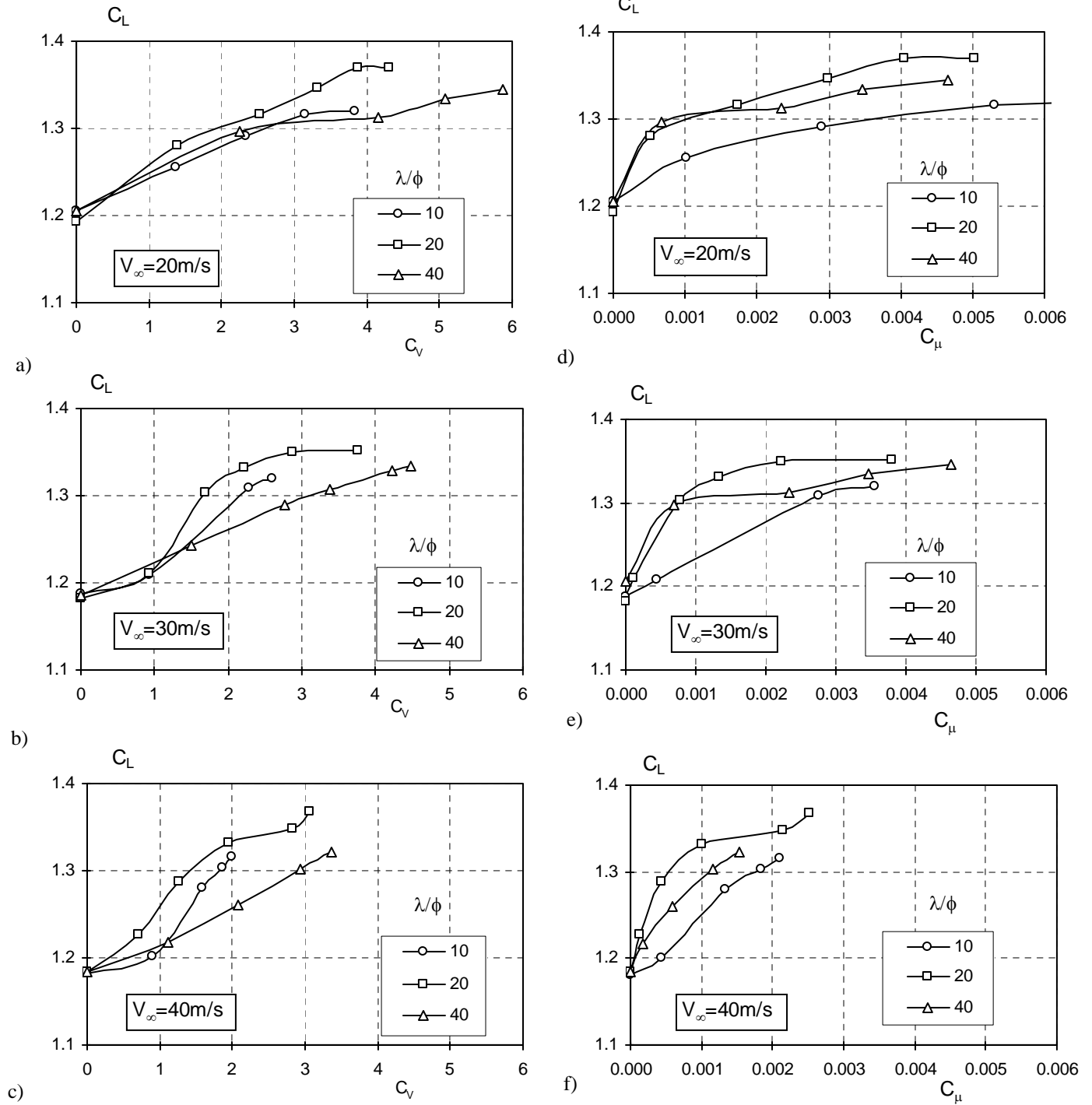
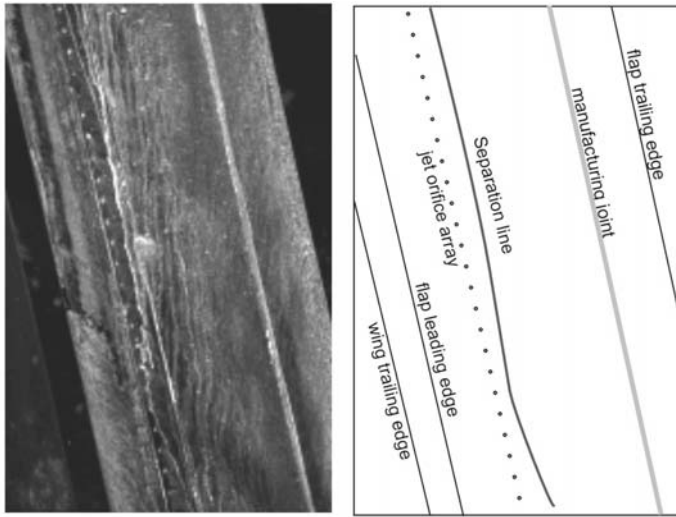
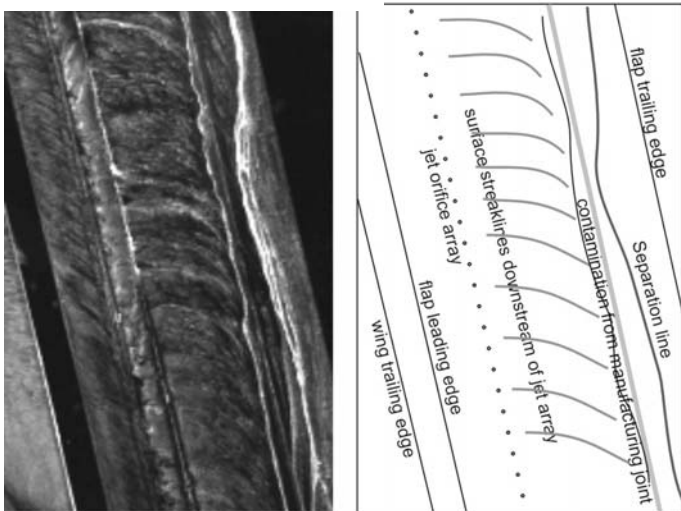


Figure 11 Effect of orifice spacing on lift recovery. LH column, C_L plotted against jet velocity ratio, RH column, C_L plotted against jet momentum coefficient. DLG = [37 0 3.5], $\alpha = 0^\circ$. Orifice diameter 0.5mm.



a) Baseline (no blowing)



b) Blowing on, $C_v = 2.6$

Figure 12 Surface oil flow visualization of the flow over the upper surface of the flap comparing the separation location for blowing on and blowing off. $DLG=[37.5 \ 0 \ 3.5], \alpha = 0^\circ, V_\infty = 30\text{m/s}$. Flow left to right.

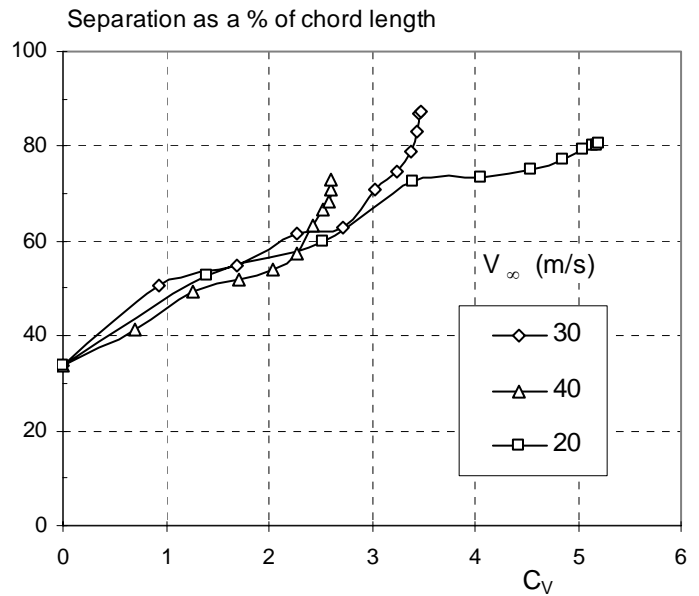
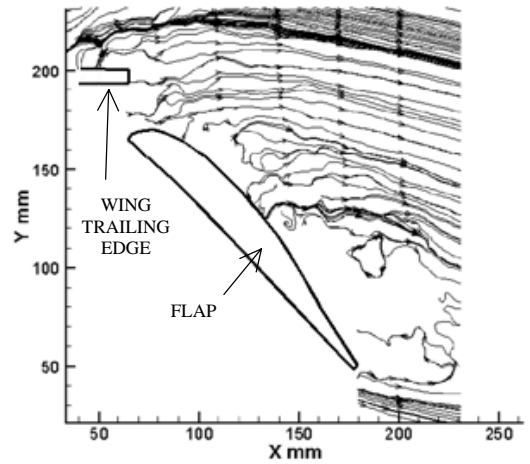
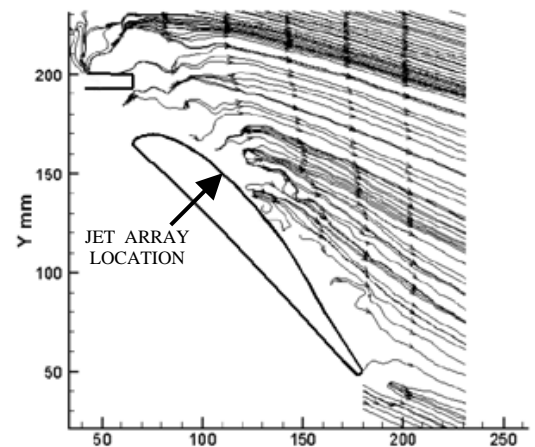


Figure 13 Flap upper surface separation location as a function of jet velocity ratio for a range of free stream speeds



a) Baseline (no blowing)



a) Blowing on, $JVR = 2.6$

Figure 14 Effect of blowing on upper surface streamlines in the vicinity of the trailing edge flap. Streamlines computed from PIV data. $DLG=[37.5 \ 0 \ 3.5], \alpha = 0^\circ, V_\infty = 30\text{m/s}$.